

# Degassing of Medical Powder Plastics in Fused Deposition 3D Printing <sup>†</sup>

Tzu-Han Chao and Chuan-Chieh Liao <sup>\*</sup>

Department of Mechanical Engineering, Chung Yuan Christian University, Taoyuan 32023, Taiwan

<sup>\*</sup> Correspondence: chuanchiehliao@cycu.edu.tw<sup>†</sup> Presented at the 3rd IEEE International Conference on Electronic Communications, Internet of Things and Big Data Conference 2023, Taichung, Taiwan, 14–16 April 2023.

**Abstract:** Compared with traditional manufacturing methods, 3D printing is designed according to the needs of patients at a lower cost. Therefore, it has recently been developed vigorously in the application of medical equipment. The printing of biomedical materials with powder plastic (PEG-PCL) in the form of fused deposition modeling is one of the most recent key development projects. In this method, the plastic was heated and melted at the nozzle of the bucket and then printed. However, due to the existence of voids between the particles, the powder was melted, and the gas was coated in the melt. Due to the high viscosity of the melt, the air bubbles could not escape freely depending on the density difference, which led to a discontinuous plastic output during the printing process and, in turn, affected the appearance and material strength of the printed product. In this study, the Volume of Fluid method was used to simulate the rising process of bubbles in the molten liquid. By studying the internal flow of the liquid, the influence of the viscosity of different fluids on the rising of bubbles was discussed. In addition, the reliability of the simulation results was obtained through experimental verification. In the future, the rotating conical agitator should be used to generate forced convection inside the liquid to accelerate a rise in bubbles, and the influence of the conical agitator on the rise of bubbles at various speeds needs to be further studied. Finally, a suitable speed range was found for the most effective degassing effect.

**Keywords:** biomedical material; 3D printing; fused deposition modeling (FDM); degassing

**Citation:** Chao, T.-H.; Liao, C.-C.Degassing of Medical Powder Plastics in Fused Deposition 3D Printing. *Eng. Proc.* **2023**, *38*, 69. <https://doi.org/10.3390/engproc2023038069>

Academic Editors: Teen-Hang Meen, Hsin-Hung Lin and Cheng-Fu Yang

Published: 30 June 2023



**Copyright:** © 2023 by the authors. Licensee MDPI, Basel, Switzerland. This article is an open access article distributed under the terms and conditions of the Creative Commons Attribution (CC BY) license (<https://creativecommons.org/licenses/by/4.0/>).

## 1. Introduction

The development of 3D printing technology was made to cope with the advantages of complex structures and rapid manufacturing so that fields of application could continue to increase. PEG-PCL is a biocompatible plastic [1]. It is manufactured by 3D printing and applied to medical equipment to design and print what is needed for patient treatment. Because it needs to be implanted into human tissue, the material requires good biocompatibility. This material is used to build a biocomposite scaffold for bone cell tissue to treat cartilage tissue with poor self-repairing ability. Due to the characteristics of the material, it cannot be pressed into a thin wire shape that is convenient for feeding; therefore, it needs to be heated and melted before printing.

There are several types of 3D printing, and the appropriate printing method can be selected according to different needs. Jihua et al. [2] listed several common types, such as fused deposition modeling, powder bed inkjet printing, stereolithography, and selective laser sintering. Fused deposition modeling sends the polymer plastic into the nozzle, heats it into a semi-liquid state, extrudes it to the top of the platform to form layer by layer, and then cools and solidifies. Powder bed inkjet printing has a liquid binder on the powder through a nozzle to form a pattern. The printing methods of stereolithography and selective laser sintering both polymerize or melt powder materials in the form of a laser. This report cites the existing fused deposition modeling printers for biomedical materials. Plastic

PEG-PCL is available in powder form. During the preheating process, the air is surrounded by particles during the melting process, causing bubbles to form inside the barrel. Due to the high viscosity of the material, the density difference does not help air bubbles escape from the molten liquid, as shown in Figure 1. These air bubbles affect the printing process and the quality of the molded product. Therefore, a suitable degassing operation needs to be selected to improve the print quality.

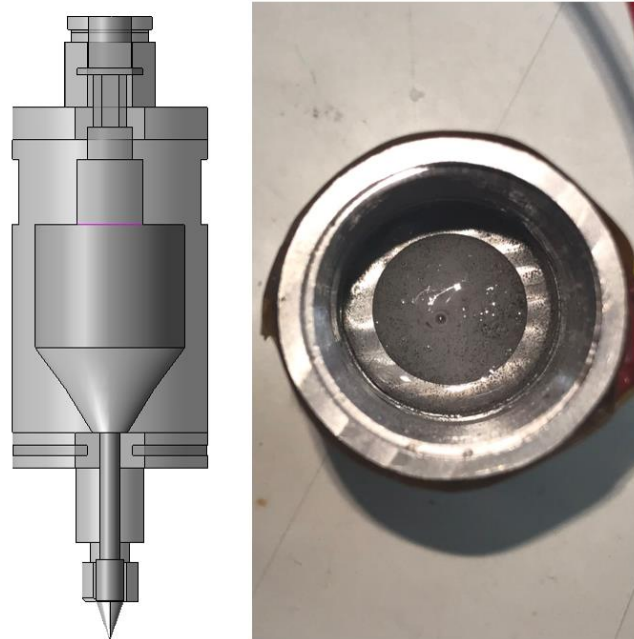


**Figure 1.** The 3D printer structure and bubble problems.

There are many examples of current 3D printing practices that are used in medical equipment, but there is little research on the problem of bubbles in the melting of medical plastics in the barrel despite the fact that these bubbles can easily affect the quality of the finished product. There are many degassing problems of high-viscosity fluids in the industrial field, and these degassing methods include a chemical clarifying agent, ultrasonic degassing, low-frequency vibrations, purging gas, blade stirring, and rotary stirring [3–6].

However, these bubbles come from the gaps between plastic particles, which are encapsulated by a high viscous force during the melting process. They do not need to rely on the cavitation pressure difference generated by the purge gas or ultrasonic vibration to release the dissolved gas molecules. Powder plastics are a form of medical equipment; therefore, it is not advisable to use excessively high temperatures to increase the circulating convection or add clarifying agents to it.

In terms of numerical models, Xu et al. [7] used axisymmetric simulations to simulate the bubbles breaking through the surface of the molten metal, which coincided with the experimental results. Moreover, Xu et al. [8] used VOF to simulate the bubbles in water and verified its feasibility from the average velocity and experiments.

Maniruzzaman et al. [9] used axisymmetric geometry to simulate the flow patterns, bubble distribution, inclusion trajectories, and turbulent flow structures in a ladle. Kunciewicz et al. [10] used a 3D/2D mixing model to simulate the operation of the blade in laminar flow. Based on dividing the entire mixer space into two regions, the velocity distribution was determined based on the model, which was in good agreement with the experiment. Therefore, it is feasible to use a 2D model to simulate the rotating flow field.

Researchers have carried out degassing research on air bubbles in 3D printing material barrels. However, there are many ways to apply degassing in the industry. We used a cone stirrer to form forced convection and accelerate the rise in air bubbles while reducing air bubbles during printing. In order to reduce this computational complexity,

a two-dimensional axisymmetric model was used to establish a two-phase mathematical model and simulate the movement behavior of bubbles in the degassing unit.

### 2. Geometric Description

The powdered plastic was placed inside the barrel, preheated, and melted through the heater on the wall surface. Then, the heat source was transferred inward from the wall surface, which coated the air that had not been diffused in the particle. In the axisymmetric simulation, a two-dimensional geometric model is shown in Figure 2. The height of the bucket was 0.04 m, the symmetrical width was 0.01 m, and the depth of the conical agitator was 0.01 m. The rotation radius was 0.0025, 0.005, and 0.0075 m, respectively.

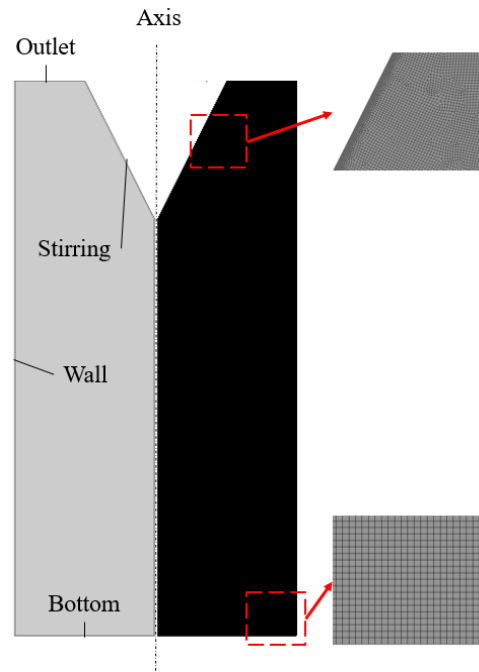


Figure 2. Simulation geometry and mesh.

### 3. Governing Equation

In this model, the flow behavior of the bubbles in the melt was predicted by numerically solving the governing equations. Both the gas phase and the liquid phase obeyed the continuity equation; the momentum equation is called the Navier–Stokes equation. The continuity equation is shown as follows:

$$\nabla \cdot (\rho \vec{u}) = 0 \tag{1}$$

where the non-rotating momentum equations are:

$$\begin{aligned} & \frac{\partial}{\partial t}(\rho u) + \frac{1}{r} \frac{\partial}{\partial x}(r \rho u^2) + \frac{1}{r} \frac{\partial}{\partial r}(r \rho u v) \\ & = -\frac{\partial p}{\partial x} + \frac{1}{r} \frac{\partial}{\partial x}[r \mu (2 \frac{\partial u}{\partial x})] + \frac{1}{r} \frac{\partial}{\partial r}[r \mu (\frac{\partial u}{\partial r} + \frac{\partial v}{\partial x})] + \rho g_x + F_x \end{aligned} \tag{2}$$

$$\begin{aligned} & \frac{\partial}{\partial t}(\rho v) + \frac{1}{r} \frac{\partial}{\partial x}(r \rho u v) + \frac{1}{r} \frac{\partial}{\partial r}(r \rho v^2) \\ & = -\frac{\partial p}{\partial x} + \frac{1}{r} \frac{\partial}{\partial r}[r \mu (2 \frac{\partial v}{\partial r})] + \frac{1}{r} \frac{\partial}{\partial x}[r \mu (\frac{\partial u}{\partial r} + \frac{\partial v}{\partial x})] - 2\mu \frac{v}{r^2} + \rho \frac{\omega^2}{r} + \rho g_r + F_r \end{aligned} \tag{3}$$

where  $u$  is the axial velocity,  $v$  is the radial velocity,  $x$  is the axial coordinate,  $r$  is the radial coordinate,  $p$  is the pressure in the fluid domain, and  $\omega$  is the swirl velocity.

$F$  represents the surface tension per unit volume between the air and water. The surface tension source term in the momentum equation could be defined as:

$$F = \sigma \frac{\rho \kappa \nabla \alpha}{0.5(\rho_l + \rho_g)} \tag{4}$$

where  $\sigma$  is surface tension;  $\kappa = \nabla \times \hat{n}$ ,  $\hat{n} = \frac{n}{|n|}$ ; and  $n = \nabla \alpha$ .

The VOF model introduced each mesh into the volume fraction of each phase. The volume fractions of all phases were then added to the units in the control volume. Combined with the laminar flow, this method had the advantages of easy implementation and high accuracy. If  $\alpha$  corresponds to the liquid volume fraction, the phases and interface could be determined by the following definitions.

$$\begin{cases} \alpha = 0 & , \text{ stands for gas phase} \\ 0 < \alpha < 1 & , \text{ stands for interface} \\ \alpha = 1 & , \text{ stands for liquid phase} \end{cases}$$

The transport equation of each volume fraction  $\alpha_1$  and  $\alpha_2$  in an incompressible two-fluid system is given by:

$$\frac{\partial \alpha_i}{\partial t} + \nabla \cdot (\vec{u} \alpha_i) = 0, \quad i = 1, 2 \tag{5}$$

with  $u_i$  being the velocity of component  $i$ .

Based on the volume fraction, the density and viscosity in the mixing zone were calculated by:

$$\rho = \rho_l \alpha + \rho_g (1 - \alpha) \tag{6}$$

$$\mu = \mu_l \alpha + \mu_g (1 - \alpha) \tag{7}$$

#### 4. Numerical Validation

In order to calculate this partial differential equation, a two-dimensional axisymmetric model was established. The equations were discretized by the finite volume method. The coupling term of pressure and velocity adopted the PISO algorithm in a transient simulation. In discrete governing equations, the pressure term used the PRESTO! (PREssure STaggering Option) scheme. The momentum term adopted QUICK (Quadratic Upwind Interpolation for convection Kinetics). The volume fraction term was Geo-Reconstruct.

Before the numerical simulation, we verified the correctness of selecting the VOF model for calculation. In Figure 3, Li et al. [11] studied the rising deformation of bubbles in glycerol. The bubbles in glycerol showed a change of 61.23% from the sphere to the ellipse gradually. The fluid properties in this study refer to the rising process of bubbles under 100% glycerol, in which the viscosity of 100% glycerol was 1.407 kg/ms, which is a thousand times higher than that of water.

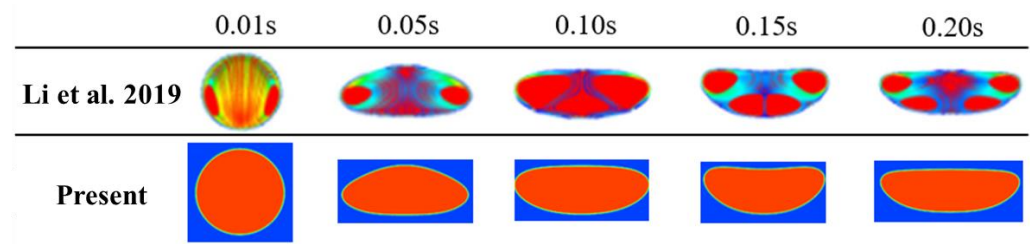
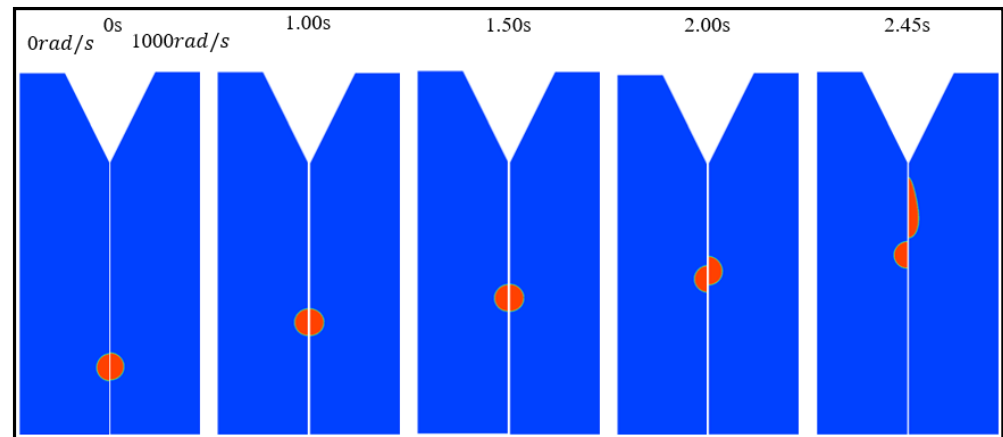


Figure 3. Deformation process of a single central circular bubble [11].

## 5. Result and Discussion

High viscous forces slow the fluid flow, which, in turn, causes the bubbles to rise slowly. The most direct way is to make the fluid produce forced convection to guide the bubble to accelerate upward. At first, the bubbles were not significantly affected because they were at a certain distance from the cone agitator and maintained a steady rise. As shown in Figure 4, the position map of the bubbles with and without rotation speeds are compared at different times. When the air bubbles entered the influence range of the agitator, the distance between the rotating cone and the air bubbles at no rotation speed gradually increased.



**Figure 4.** Comparison of bubbles at different time points at 1000 rad/s and no rotation speed.

In the viscosity fluid, the cone agitator drove the flow of the liquid. Due to the centrifugal force generated by the rotation, forced convection was formed in the fluid with the center upward and the upper edge of the bubble closer to the cone. The faster flow and viscosity of the original fluid made the bubbles gradually take on the shape of water droplets.

### 5.1. Rotation Speed Effect

In the case of different rotational speeds, the effect of convection on the air bubbles increased. As shown in Figure 5, the horizontal axis and the vertical axis, represented the position of the bubbles, which rose at different times. When the stirring radius of the bubbles was 5 mm, the positions of the bubbles were at different speeds. As the rotation speed increased, this effect became obvious, but the height of the bubbles rose only in the later stage. This was because the influence range of stirring was still limited by the viscosity. Therefore, when the bubbles rose to the influence range obvious effect, the distance that the bubbles moved in 2 s and 2000 rad/s increased by 7.3% compared with no rotation speed under the action of increasing the rotation speed. With the increase in the rotation effect, it increased to 13% at 2.2 s. The increase in the rotational speed had the effect of increasing the bubbles.

### 5.2. Rotation Radius Effect

At a fixed rotational speed, different rotation radius changes took place. As shown in Figure 6, under the rotation speed of 1000 rad/s and the influence of a different radius, the position of bubbles at each time varied. At the minimum rotation radius of 0.0025 m (2.5 mm), the convection effect caused by the rotation radius was small, and the curve observed on the ascent height map was closer to that without rotation. In the observation at 2 s, when the rotation radius of the bubble increased, the rotation radius of the bubble increased to 0.0075 m (7.5 mm), and the distance that the bubble moved was 13.4% higher than that of the bubble without rotation. Figure 7 shows that the bubbles rose under the influence of a different stirring radius at 2 s.

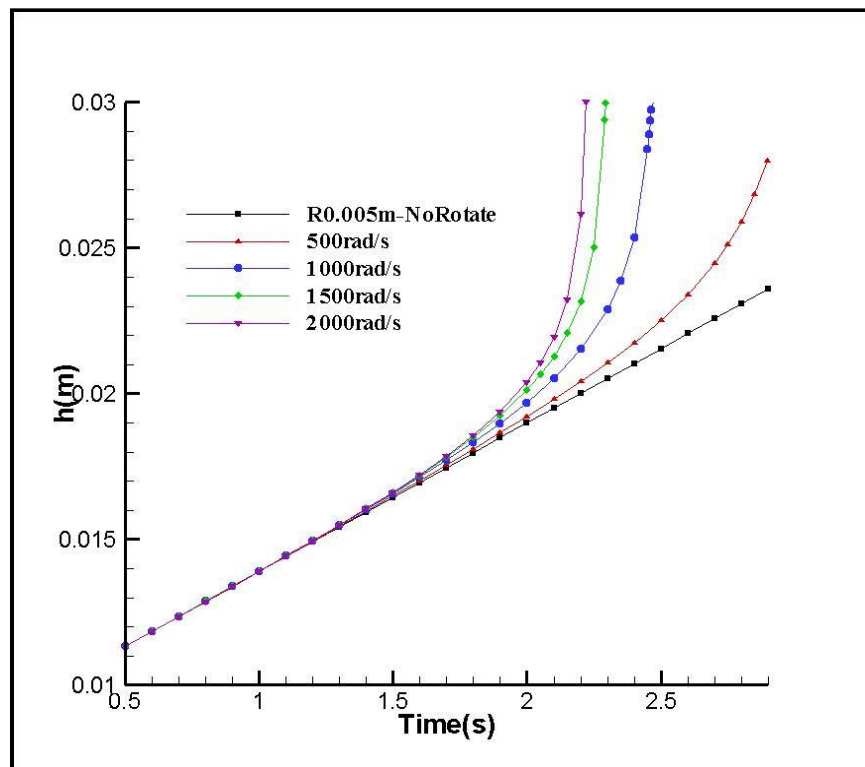


Figure 5. Height of bubbles rising at different rotational speeds.

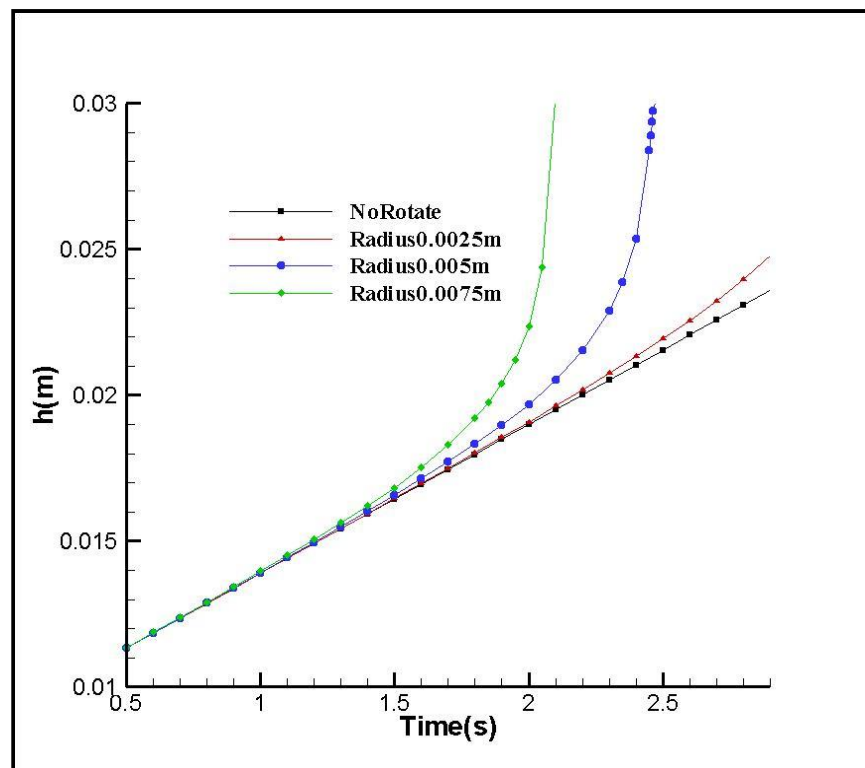
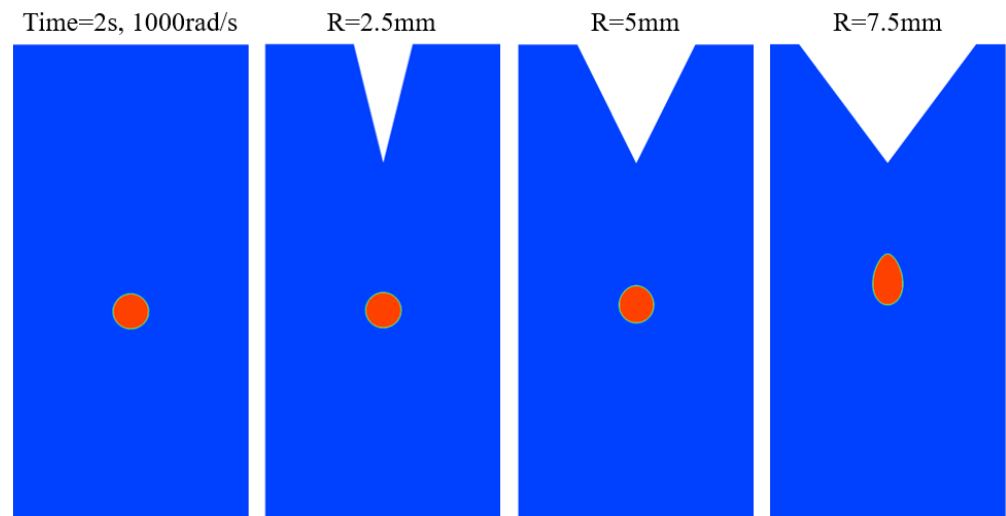


Figure 6. Effect of different radius at speed of 1000 rad/s.



**Figure 7.** Effect of a different stirring radius at 2 s.

## 6. Conclusions

VOF can be used to simulate the flow of bubbles in the viscous fluid, and the effect of bubbles rising was observed through the influence of the agitator. The influence of the cone agitator on the bubbles was studied, including the speed of the agitator (500–2000 rad/s) and the size (5–7.5 mm). At 2s, the rotation speed increased under the fixed rotation radius (5 mm). When the bubble's rising speed increased, the moving distance increased by 13%. At a fixed rotation speed (1000 rad/s), the moving distance of the bubble with a large rotation radius increased by 13.4%, which showed the effect of the cone agitator on the bubble rise gain. Subsequently, this cone-stirring model was applied to a higher-viscosity fluid. In addition to observing the effect on the bubbles, the rotation radius and depth of the cone were changed at the same time, and the volume of the cone was controlled at the minimum proportion to obtain the maximum effect.

**Author Contributions:** T.-H.C.: Validation, Investigation, Data curation, Writing—original draft preparation, Visualization; C.-C.L.: Conceptualization, Methodology, Formal analysis, Investigation, Resources, Writing—original draft preparation, Writing—review and editing, Supervision, Project administration, Funding acquisition. All authors have read and agreed to the published version of the manuscript.

**Funding:** This research was funded by the Ministry of Science and Technology (MOST 110-2221-E-033-016, MOST 111-2221-E-033-031).

**Institutional Review Board Statement:** Not applicable.

**Informed Consent Statement:** Not applicable.

**Data Availability Statement:** Not applicable.

**Acknowledgments:** This research was funded by the Ministry of Science and Technology, Taiwan, ROC via Grant Nos. MOST 110-2221-E-033-016 and MOST 111-2221-E-033-031.

**Conflicts of Interest:** The authors declare no conflict of interest.

## References

1. Hsieh, Y.H.; Shen, B.Y.; Wang, Y.H.; Lin, B.; Lee, H.M.; Hsieh, M.F. Healing of osteochondral defects implanted with biomimetic scaffolds of poly ( $\epsilon$ -caprolactone)/hydroxyapatite and glycidyl-methacrylate-modified hyaluronic acid in a minipig. *Int. J. Mol. Sci.* **2018**, *19*, 1125. [[CrossRef](#)] [[PubMed](#)]
2. Wang, X.; Jiang, M.; Zhou, Z.W.; Gou, J.H.; Hui, D. 3D printing of polymer matrix composites: A review and prospective. *Compos. Part B Eng.* **2017**, *110*, 442–458. [[CrossRef](#)]
3. Zhan, X.; He, Y.; Shen, B.; Sun, Z.; Shi, T.; Li, X. Removal of gas bubbles from highly viscous non-Newtonian fluids using controlled vibration. *Chem. Eng. Sci.* **2018**, *185*, 76–83. [[CrossRef](#)]

4. Liu, X.; Zhang, Z.; Hu, W.; Le, Q.; Bao, L.; Cui, J.; Jiang, J. Study on hydrogen removal of AZ91 alloys using ultrasonic argon degassing process. *Ultrason. Sonochem.* **2015**, *26*, 73–80. [[CrossRef](#)] [[PubMed](#)]
5. Gómez, E.R.; Zenit, R.; Rivera, C.G.; Trápaga, G.; Ramírez-Argáez, M.A. Mathematical Modeling of Fluid Flow in a Water Physical Model of an Aluminum Degassing Ladle Equipped with an Impeller-Injector. *Met. Mater. Trans. B* **2012**, *44*, 423–435. [[CrossRef](#)]
6. Ma, Q.; Li, C.; Zhang, G.; Fang, H. A novel method for accelerating bubble rising in highly viscous molten quartz. *Int. J. Heat Mass Transf.* **2019**, *138*, 1359–1367. [[CrossRef](#)]
7. Xu, Y.; Ersson, M.; Jönsson, P. Numerical Simulation of Single Argon Bubble Rising in Molten Metal Under a Laminar Flow. *Steel Res. Int.* **2015**, *86*, 1289–1297. [[CrossRef](#)]
8. Xu, Y.; Ersson, M.; Jönsson, P.G. A Numerical Study about the Influence of a Bubble Wake Flow on the Removal of Inclusions. *ISIJ Int.* **2016**, *56*, 1982–1988. [[CrossRef](#)]
9. Maniruzzaman, M.; Makhlouf, M. Mathematical modeling and computer simulation of the rotating impeller particle flotation process: Part I. Fluid flow. *Met. Mater. Trans. B* **2002**, *33*, 297–303. [[CrossRef](#)]
10. Kunczewicz, C.; Rieger, F.; Pietrzykowski, M.; Stelmach, J. 3D/2D hybrid model for ribbon impellers operating in laminar regime. *Chem. Eng. Process. Process. Intensif.* **2013**, *73*, 50–58. [[CrossRef](#)]
11. Li, X.; Zhang, P.; Li, J.; Wang, W.; Chen, G. Analysis of deformation and internal flow patterns for rising single bubbles in different liquids. *Chin. J. Chem. Eng.* **2019**, *27*, 745–758. [[CrossRef](#)]

**Disclaimer/Publisher’s Note:** The statements, opinions and data contained in all publications are solely those of the individual author(s) and contributor(s) and not of MDPI and/or the editor(s). MDPI and/or the editor(s) disclaim responsibility for any injury to people or property resulting from any ideas, methods, instructions or products referred to in the content.